Mine Water Environ (2016) 35:243–252
DOI 10.1007/s10230-016-0385-5

TECHNICAL ARTICLE

Numerical Simulation of Water Flow from the Coal Seam Floor in a Deep Longwall Mine in China

Huiyong Yin[1,2] · Jiuchuan Wei[1] · Liliana Lefticariu[3] · Jianbin Guo[1] · Daolei Xie[1] · Zilin Li[4] · Peng Zhao[4]

Received: 18 March 2015 / Accepted: 20 January 2016 / Published online: 1 February 2016

Abstract The study of groundwater flow from the coal seam floor is critical to safe mining operations in China. We developed a numerical simulation model to describe flood water pathways during mining, using the field conditions present at the no. 4196 west work face in the Panxi longwall coal mine, Shandong Province, China, Groundwater flow analysis revealed unusual values for the failure depth of the coal seam floor. The high ground stress and underground pressure, excavation length, width of working face, poor mechanical properties of aquitards, and expansion of fractures by groundwater infiltration all contribute to groundwater flow into the mine. The modeling results predict the time and longwall locations associated with the maximum likelihood of flood occurrence. Such results can be used by decision makers to improve mine design and safety.

Keywords Groundwater inflow · Failure depth of coal seam floor · Damage zone · Shear stress-fracture

✉ Huiyong Yin
yhy1919@163.com

[1] State Key Laboratory of Mining Disaster Prevention and Control, College of Earth Science and Engineering, Shandong University of Science and Technology, Qingdao 266590, China

[2] College of Geoscience and Surveying Engineering, China University of Mining and Technology, Beijing 100083, China

[3] Department of Geology, Southern Illinois University, Carbondale, IL 62901, USA

[4] Wanxiang Mining Co., Ltd, Laiwu 271109, China

Introduction

Many coal mine flooding accidents have occurred in China during the past few decades, causing serious economic loses and many fatalities (Huang et al. 2014a, b; Jin et al. 2011; Li et al. 2014; Wang et al. 2012b; Wu et al. 2011, 2013). The risk of flooding generally increases with mining depth and water pressure on the mine floor (Gu et al. 2010; Wang and Park 2003). The North China Coal Basin is a major coal producing region in China. Due to the scarcity of shallow coal reserves there, most coal mines are operating at great depth, which increases ground stress, temperature, karst water pressure, and mining disturbance (He et al. 2005), and contributes to coal seam floor failure and flooding by water from the Ordovician limestone aquifer, which is a confined karst aquifer that contains an abundant supply of water and very high water pressure (Zhang 2005). Therefore, detailed knowledge on the factors that contribute to coal seam floor failure and flooding during mining are needed.

Water sources, water volume, and flow paths have always been of interest for engineers and professionals that work at preventing failure of the coal seam floor and flooding during mining. When mining the working face, the stress field in the rock mass below the coal seam is changed; new fractures develop, which can change the strength of the rock mass (Yang et al. 2007). The new fractures combine with natural fissures and can create new groundwater flow paths. Moreover, the flowing groundwater can also contribute to fracture propagation.

Theoretical field models, numerical models, and physical analogs have been used to analyze the deformation and failure of the rock mass in the floor of coal seams at working faces (Li et al. 2013; Yang et al. 2007). Although these studies have shown that the failure depth of coal seam

floor increases with mining depth (Jiang 2009), there is still a limited understanding of groundwater flow paths prior to flooding, especially in deep longwall mines.

The main methods of testing the depth of deformation and failure of the coal seam floor include hydraulic fracturing, acoustic waves, radio-wave penetration, ultrasonic imaging, numerical simulations, and strain sensor monitoring (Zhu et al. 2014). Numerical simulation, which can depict the progress of groundwater flow paths under high stress conditions, is also used to determine the stress and deformation during mining (Li et al. 2013; Mahdi and Charliec 2012; Yang et al. 2011). Various software, such as FLAC, UDEC/3DEC, ANSYS, COMSOL, RFPA, are now capable of accounting for complex material behaviors (Yang et al. 2011).

The main objective of this research was to address how water flow paths evolve from the coal seam floor during mining. The goals of this study were to:

- present a complete development of fracture generation, extension, broadening, and coalescence during mining,
- understand the main factors that affect fracture development in the coal seam floor, and
- predict the most vulnerable place and time of rock failure and groundwater inflow in a deep longwall mine.

In this paper, we first discuss the characteristics of abnormal failure depth of the coal seam floor in a deep coal mine, then depict groundwater flow from a high-pressure confined aquifer into a coal seam, and then finally explore the spatial and temporal hazards associated with longwall mining. A better understanding of groundwater flow during longwall mining in deep mines should allow decision makers to minimize the negative effects of coal mine flooding on worker safety and mine productivity.

Study Area

Overview of the Panxi Coal Mine

The Panxi Mine is located south of Laiwu, Shandong Province, eastern China (Fig. 1). It lies in the eastern portion of the Laiwu coal field, covers an area of 13.9 km^2, and has an annual coal production of one million tonnes. From top to bottom, the stratigraphic succession consists of Quaternary, Paleogene, Jurassic, Permian, Carboniferous, and Ordovician strata. The coal seams are located in the Carboniferous-Permian formations. The main minable seam is the no. 19, which belongs to the Taiyuan formation (Pennsylvanian). Longwall mining is employed with backward extraction. The coal seam has a monoclinal structure with a strike of 290°–320° and a northeast dip of about 23°. The main strike faults are divided into three groups, with directions of NW, E–W, and S–N. The main aquifers are the Quaternary gravel, Paleogene conglomerate, Jurassic red sandstone, Permian sandstone, Taiyuan sandstone, and Carboniferous and Ordovician limestones. The confined Ordovician limestone aquifer is responsible for groundwater-related disasters during excavation of the no. 19 coal seam. Twenty-three groundwater-related incidents have been recorded since 1960, when the Panxi Mine became active. Five of these were not induced by known natural faults but resulted from failure of the coal seam floor and other factors associated with mining (Table 1).

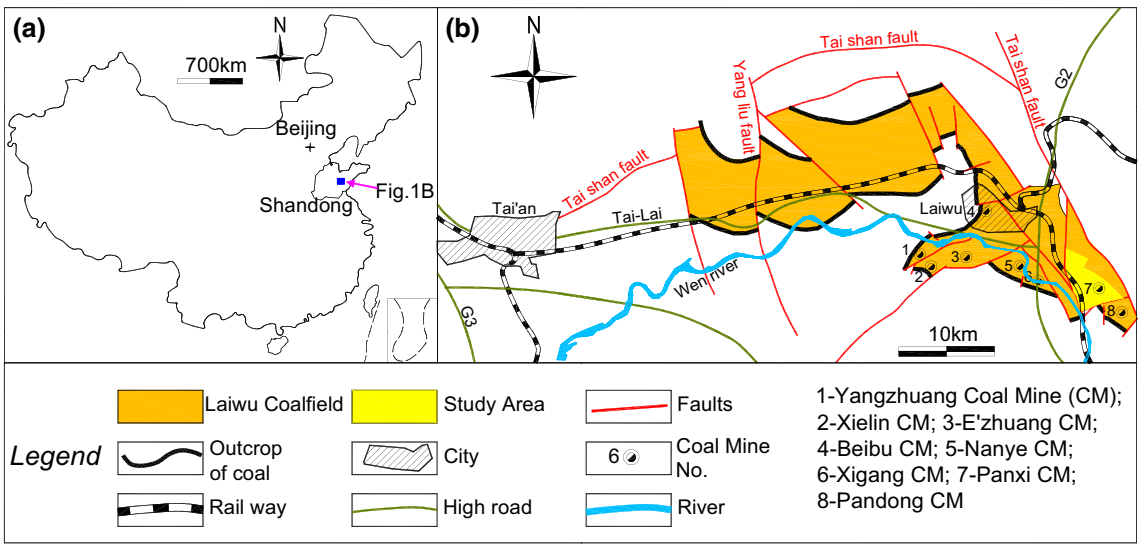

Fig. 1 Location of the Panxi coal mine

Table 1 Mining and hydrological parameters of water inflow incidents recorded in the Panxi coal mine, which led to flooding by the groundwater from the Ordovician limestone aquifer

No.	Time	Elevation (m)	Water pressure (MPa)	Max. flow rate (m^3/h)	Note
1	11-29-1998	−407	\	240	No information
2	01-19-2001	−490	4.8	310	Area of palaeokarst
3	03-08-2001	−490	4.8	600	Area of palaeokarst
4	04-06-2003	−612.4	5.1	750	Area of palaeokarst
5	24-12-2004	−656.9	5.1	336	Area of rich water capacity (Fig. 3)

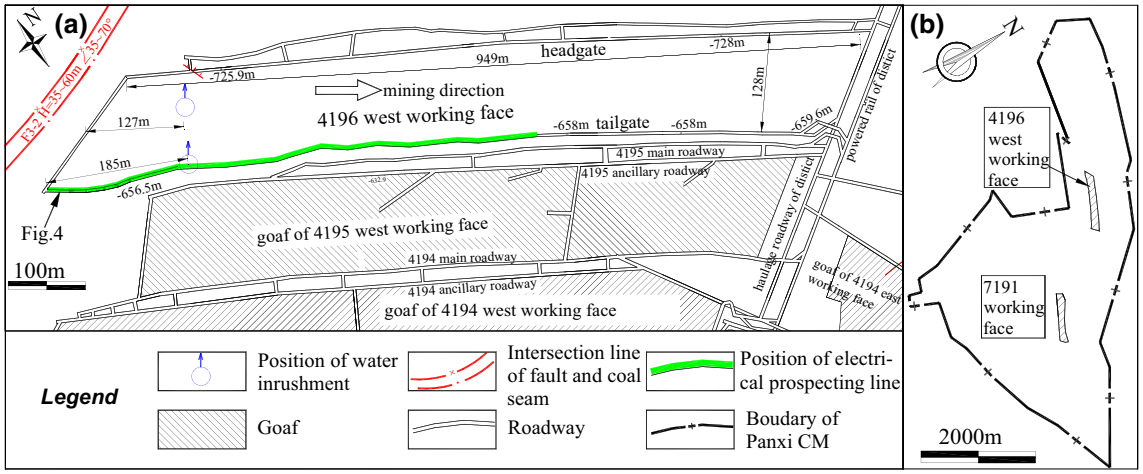

Fig. 2 Position of water inrush in the 4196 west working face and 7191 working face

Geological and Hydrogeological Conditions at the 4196 West Working Face

The no. 4196 west working face is located in the NW sector of the Panxi coal mine. Its absolute elevation ranges from −656 to −730 m, and its ground elevation from +220 to +225 m, so the working face is ≈950 m below the ground surface. Figure 2, which shows part of the mine plan, indicates the position of the relevant working faces, water inrush, and electrical prospecting on the tailgate. The strike length of the working face was ≈945 m, the dip width ≈130 m, and the mining area was ≈122,850 m^2. The thickness of the no. 19 coal seam, which dips at an angle of ≈22°, ranges from 2.50 to 2.65 m, with an average of 2.55 m. The working face has a simple monoclinal structure, and the few faults were mapped by ground penetrating radar and mining operations.

The main roof of the working face consisted of a ≈17 m thick, fine-grained, silica clastic sandstone with calcite cement. The immediate roof consisted of siltstone or fine grained sandstone with a thickness of ≈8 m. The immediate floor of the working face consisted of a ≈4 m thick sandy mudstone; the main floor was composed of siltstone (≈14 m thick) and a 2 m thick limestone (Fig. 3; Table 2).

The main confined aquifers under the no. 19 coal seam are the Carboniferous Xujiazhuang (Xu) and Caobugou (Cao) limestone and the Ordovician limestone. They are separated by 22, 38 and 60 m thick mudstone and siltstone aquicludes (Fig. 3). The Xu and Cao limestones are between 7 and 9 m thick, with in situ specific capacities of 0.00875–0.013 (L/s)/m, and a water pressure of 2.1 MPa. The massive 800 m thick Ordovician limestone aquifer has a measured specific capacity of 0.0028–0.266 (L/s)/m and a water pressure of 5.1 Mpa, and is the main hazard to safe mining.

Groundwater Flow at the 4196 West Working Face

Mining of the no. 19 coal seam started in October 2004 at the 4196 west working face. After advancing for 130 m, a sudden inflow of groundwater occurred from the headgate area at 6:35 a.m. on November 24th, 2004. The initial groundwater flow rate was 50 m^3/h and it had increased to 100 m^3/h a half hour later. The flow rate continued to rapidly increase, up to 336 m^3/h at 8:50 a.m. The flood

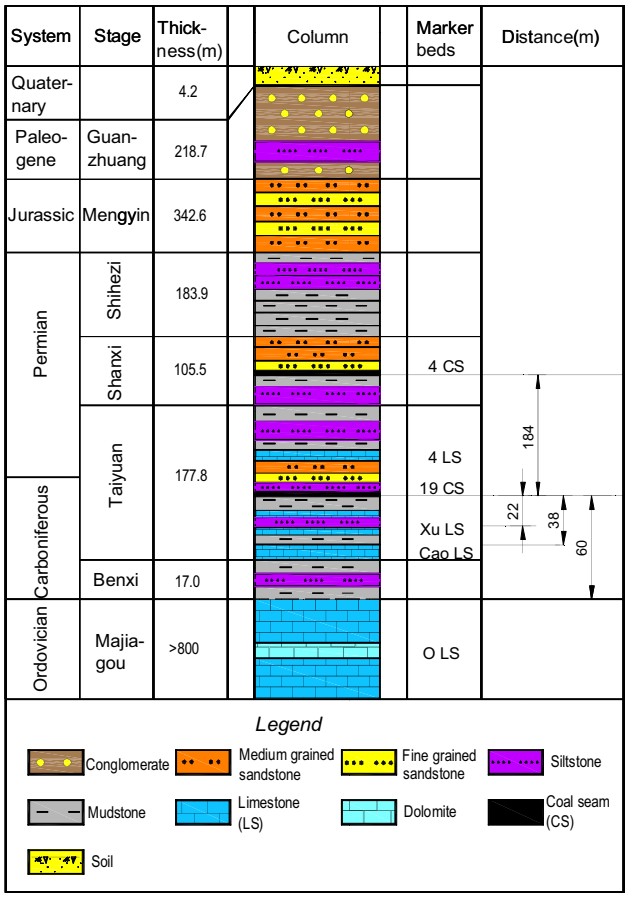

Fig. 3 Stratigraphic column of the 4196 west working face

water was clear with a temperature of 34 °C. 1 day later, the inflow decreased to 320 m^3/h, and 3 days later it stabilized at 300 m^3/h (Fig. 2a). Based on the chemical characteristics, temperature, color, volume of the inflow water, and changing water levels in the karstic Ordovician confined aquifer, it was established that this aquifer was the source of the water. Although existing faults could have acted as groundwater flow paths (Yin et al. 2007), the five flooding events listed in Table 1 were mainly caused by failure of the coal seam floor due to mining. When the rock mass under the coal seam was subjected to mechanical loading, the ground stress caused the initiation, growth, and linking of cracks. The newly fractured zone thus provided multiple pathways for groundwater flow. Once a pathway contacted the high-water pressure confined aquifer, the groundwater flooded into the excavation site. Confined aquifers can have a high water capacity and can cause prolonged and voluminous floods. Electrical prospecting along the tailgate of the 4196 west working face showed the presence of two areas with high water capacity in the Ordovician limestone (Fig. 4), where the apparent resistivity is relatively low. Groundwater inflow happened just above the area with the highest water capacity (area 1 in Fig. 4), illustrating the importance of prospecting aquifer water capacity before exploitation. In the model presented in this study, we set the hydraulic conductivity and pore-water pressure coefficient in the Ordovician limestone to a high value and used Weibull distribution parameters, due to the heterogeneous aquifer properties.

Methods

RFPA^{2D}-FLOW is a numerical software commonly used in the mining industry to display the deformation and damage of rock masses of the floor and ceiling of mined coal seams (Li et al. 2009a, b; Yang et al. 2007). It is particularly suitable for solving nonlinear large deformation problems in geotechnical and mechanical engineering (Yang et al. 2007). RFPA^{2D}-FLOW provides a variety of options for performing stress analysis, seepage analysis, coupling, and failure analysis based on the principles of continuum and damage mechanics. Coupled seepage and stress processes can be interpreted with Biot's theory of consolidation (Tang et al. 2002). Stress analysis uses the finite element method while damage analysis uses the revised Mohr–Coulomb criterion to calibrate the damaged cell parameters using the method of stiffness degradation and reconstruction (Li et al. 2009a; Tang et al. 2002). RFPA^{2D}-FLOW also provides the degradation equation of the mechanical properties of the mesoscopic unit using the mesoscopic elastic damage model. This approach uses the relationship between spatial distribution of deformation and creep acceleration and can be used to run simulations of different processes, such as creep and failure in rock mass (Li et al. 2007, 2008).

The strength and other parameters of the coal seam and surrounding rocks (Table 2) agree with test reports from the Panxi Mine and other mines in the Laiwu coal field. The mechanical properties of the rocks are heterogeneous and vary according to the Weibull distribution (Wang et al. 2012a; Yang et al. 2007):

$$w = \frac{m}{s_0}\left(\frac{s}{s_0}\right)^{m-1}\exp\left[-\left(\frac{s}{s_0}\right)^{m}\right] \quad (1)$$

where s is the mechanical parameter (Young's modulus or strength) of the elements; s_0 is the mean of parameters; m is a homogeneity index, which can be obtained from the statistical distribution of rock mass parameters with value of 1.1, 3, 5, and 7 (Wang et al. 2012a; Yang et al. 2007). A simplified 2-D numerical model was built using the RFPA^{2D}-FLOW software, taking into account the general geological, hydrogeological, spatial, and mining conditions at the 4196 west working face. The model domain was 400 m long and

Table 2 Rock mechanical parameters used in the model

Rock type	Thickness (m)	Young's modulus (MPa)	Compressive strength (MPa)	Poisson's	Internal cohesive angle (°)	Weight (N/mm^3)	Hydraulic conductivity (m/day)	Pore-water pressure coefficient
Overburden	10	20,000	200	0.12	50	5.2e−4	0.1	0.01
Med. ss	20	15,007	112	0.140	48	2.62e−5	1	0.1
Ms	5	4135	32	0.189	39	2.55e−5	0.1	0.01
No. 3 Ls	3	8717	52	0.171	46	2.65e−5	5	0.5
Silts	15	9765	67	0.173	45	2.63e−5	0.1	0.01
Ms	5	5327	38	0.186	38	2.56e−5	0.1	0.01
No. 4 Ls	7	8671	40	0.157	48	2.63e−5	5	0.5
Med.-fine ss	17	11,075	89	0.170	49	2.64e−5	0.5	0.05
Silts	8	8950	49	0.175	45	2.66e−5	0.1	0.01
No. 19 coal	3	2300	20	0.27	30	1.6e−5	0.1	0.01
Cs	4	4144	31.8	0.203	32	2.56e−5	0.1	0.01
Silts	2	7573	43	0.1715	38	2.62e−5	0.1	0.01
Ls	2	8539	41	0.1745	48.6	2.66e−5	5	0.5
Silts	12	12,067	90	0.187	49	2.67e−5	0.1	0.01
Xu ls-1	4	8697	40.5	0.147	49	2.64e−5	5	0.5
Siltstone	5	7472	45	0.164	48	2.67e−5	0.1	0.01
Xu ls-2	3	6235	35	0.175	48.7	2.67e−5	5	0.5
Ms	6	3410	28	0.210	32	2.69e−5	0.1	0.01
Cao ls	9	9326	54	0.1545	37	2.67e−5	5	0.01
Ms	4	4671	23	0.204	33	2.55e−5	0.1	0.01
Silts	5	7567	42	0.190	36	2.76e−5	0.1	0.01
Ms	8	5417	36	0.213	38	2.46e−5	0.1	0.01
Ordovician ls	43	11,207	75	0.167	48	2.66e−5	10	1

ss sandstone, *ls* limestone, *ms* mudstone, *cs* claystone, *silts* silstone

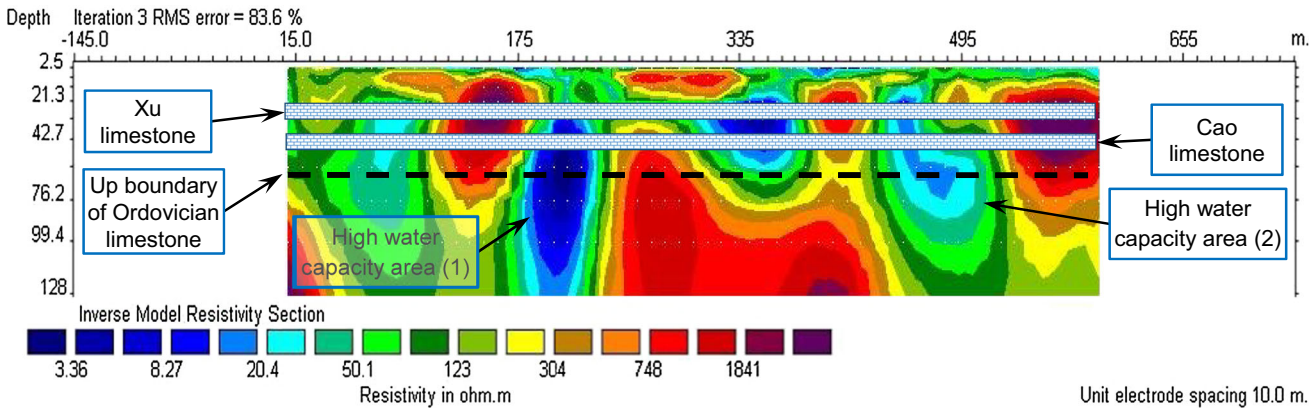

Fig. 4 Section of electrical prospecting in the tailgate (the *horizontal axis* represents distance from *left to right* side of the tailgate at the no. 4196 west working face (*wide green line* in Fig. 2) and the *vertical axis* represents the depth from the no. 19 coal seam floor)

200 m high, gridded into 80,000 elements, each with a uniform dimension of 1 m × 1 m (Table 2; Fig. 5), and contained a total of 23 layers of mudstone, limestone, siltstone, sandstone, and coal seams (Table 2; Fig. 3). A pressure of 15 MPa was applied on the top boundary as the in situ stress to simulate the vertical stress from the overburden. The bottom, left, and right boundaries were constrained in the vertical and horizontal direction, respectively.

As stated above, the Xu, Cao, and Ordovician limestone are the main confined aquifers under the coal seam floor,

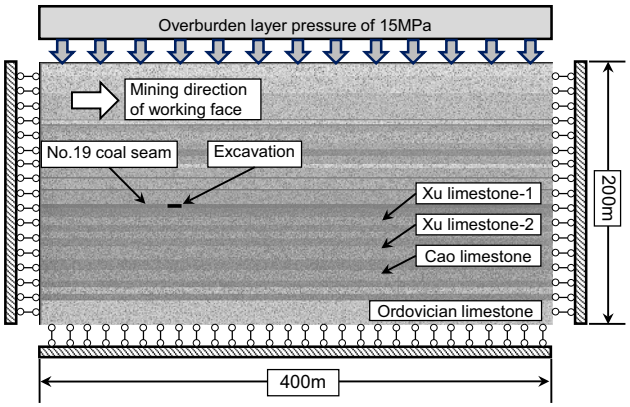

Fig. 5 Conditions used for the numerical modeling

but the Ordovician causes the most concern during mining of the no. 19 coal seam. A fluid pressure of 5.1 MPa was applied to the external boundary of the Ordovician limestone, based on the measured water level in a borehole drilled at the working face. Both the bottom and top boundaries were established as no-flow boundaries to avoid outflow from the Ordovician limestone, and the left and right boundaries were made water conductive boundaries to allow the hydraulic pressure to act on the aquifers under the coal seam floor (Fig. 5).

Results

For modeling purposes, it was assumed that the no. 19 coal seam was mined from left to right. Modeling was done with 13 steps in increments of 10 m. As mining advanced, failure occurred in the roof and floor of the no. 19 coal seam. Figure 6a–f show the shear stress distribution around the excavation space. Figure 7a–f show the elastic modulus distributions at different steps, and Fig. 8a–f show the groundwater flow rate during each mining/modeling step. When the mine face was 20 m from the left boundary (second step), the stress was focused on the excavation's immediate surroundings and the shear stress had a saddle-like pattern at the ends of the excavated passage, with a maximum value of 13.0 MPa (Fig. 6a). The shear stress increased as mining progressed, especially concentrated on both sides of the goaf space, and the distribution range on the roof was larger than on the floor. Therefore, the overlying siltstone from the immediate roof began to crack on the left side. At the same time, the floor strata were also damaged at the border between the shear stress concentration and stress relief area under the coal seam floor (Fig. 6b). When the excavation was 70 m long, the maximum shear stress increased to 26.7 MPa and the shape of the shear stress zones were like an arc at the top of overlying strata (Fig. 6c). When the mined face advanced to

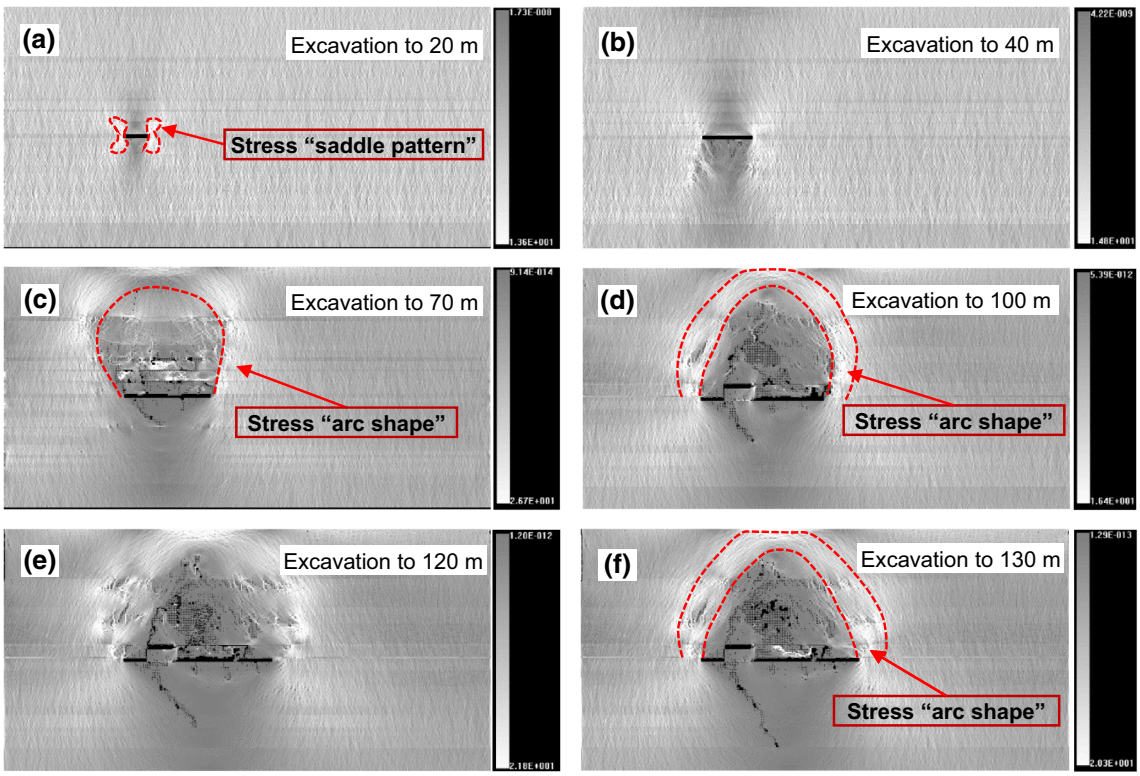

Fig. 6 Shear stress patterns and distribution

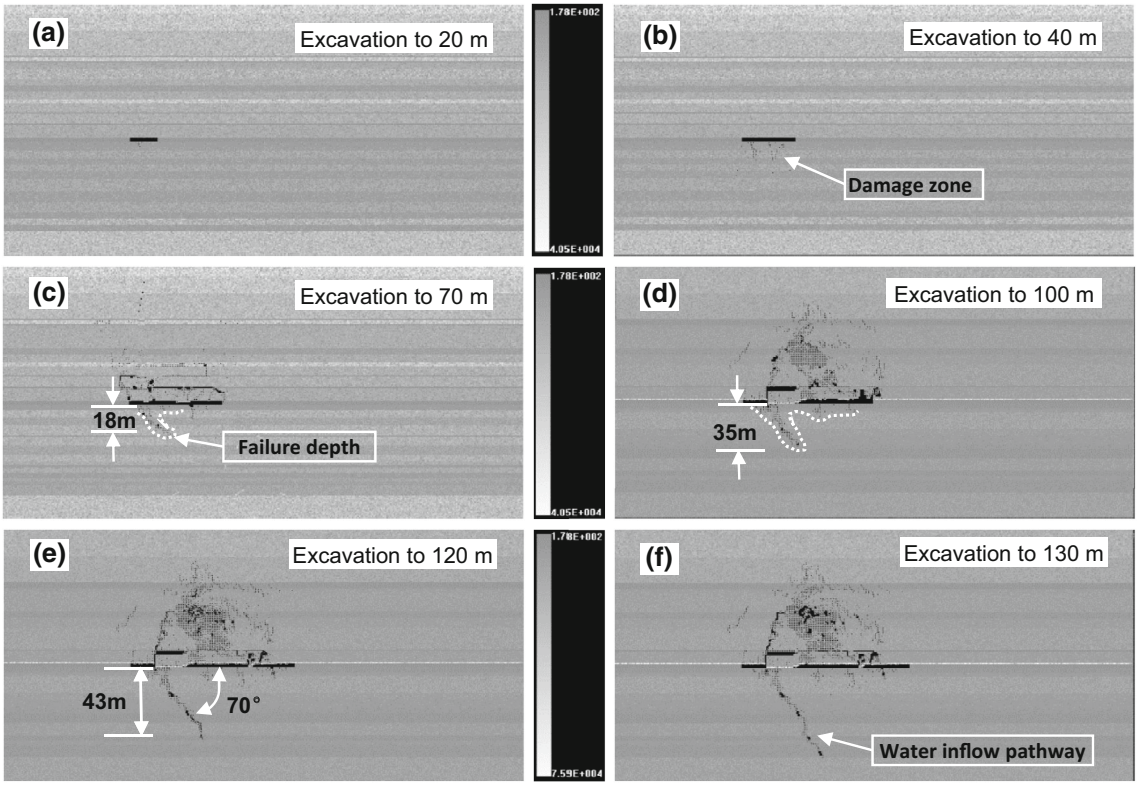

Fig. 7 Elastic modulus patterns of the roof and floor strata

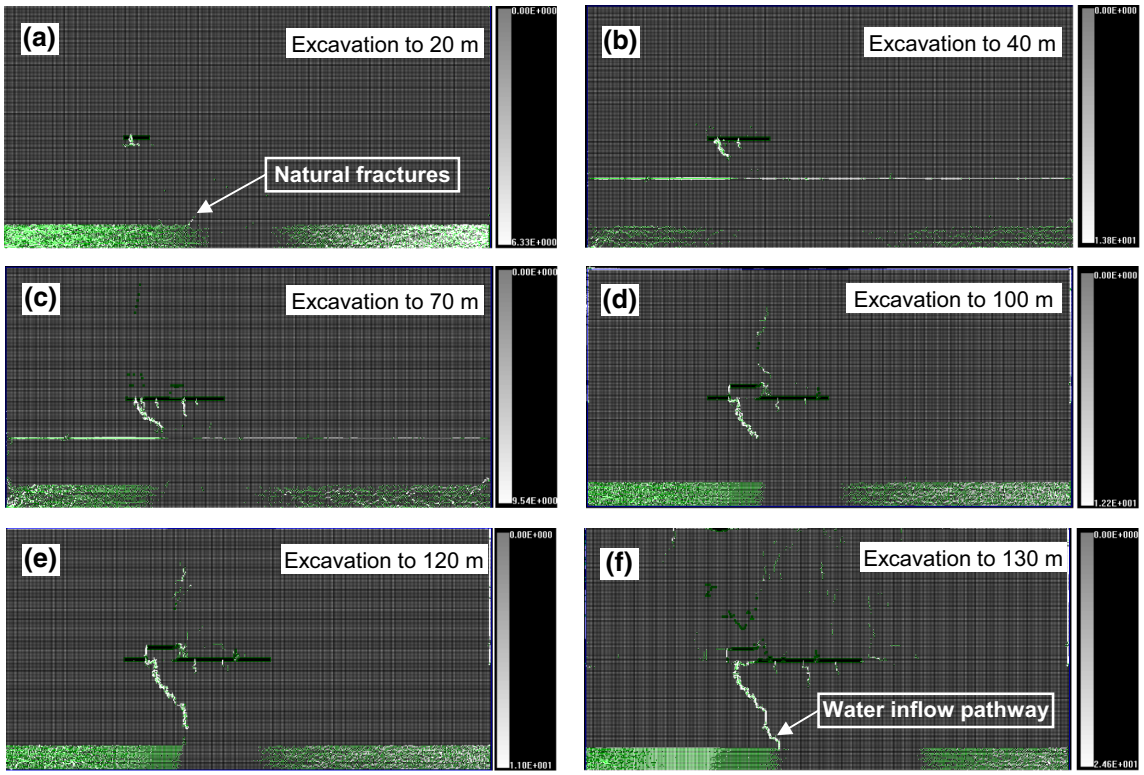

Fig. 8 Groundwater flow patterns

100 m, the maximum shear stress was mainly distributed around the roof, and the arc-like stress field around the excavation became recognizable (Xie et al. 2009), as shown in Fig. 6d. Figure 6e shows the further deformed arc-shaped stress field; the maximum height of the stress arc was about 60 m at the 12th step. When the excavation was 130 m long, the maximum shear stress was 20.3 MPa, the stress field had changed only in size, and the maximum height of the stress arc was ≈70 m (Fig. 6f).

Because of the spatially heterogeneous stress load on the floor, the strata under the coal seam floor were deformed, fractured, and damaged. Initially, the main effect of the shear stress on the mechanically weak mudstone immediately under the floor of the excavation was to produce fractures on the left side. The maximum failure depth reached ≈3 m, as shown in Fig. 7a. The damaged zone under the coal seam floor grew larger as mining progressed. The zone below the coal seam was more damaged than other areas because of the difference in mechanical properties of the rocks found at the 4th step. The simulated results in Fig. 7b suggest that the failure depth of coal seam floor was ≈8 m, where it linked with a 2 m thick limestone. The failure depth reached ≈18 m when the mining excavation was 70 m long, while the underlying impermeable rock mass remained stable, still confining the underlying aquifers (Fig. 7c). When the mining length reached 100 m, the failure depth was ≈35 m, reaching the no. 2 Xu limestone. Still, so far, the damaged zone had only created additional groundwater flow paths between the excavation and that limestone. At the 12th step, the length of floor failure had increased to ≈43 m and the dominant fracture was at an angle of ≈70° (Fig. 7e). At the 13th step, the depth of the damaged zone crossed into the Cao limestone. When the depth of the coal seam floor failure increased to ≈50 m, it reached fractures that linked it with the Ordovician limestone.

Similar to the floor strata, the roof strata also underwent deformation, fracture, damage, and collapse (Fig. 7). Before the 7th step, the immediate and main roof hardly generated fractures due to their thick and strong nature. When the excavation was 70 m long, the immediate roof began to cave and upward-extending cracks began developing in the main roof. In addition, a bed-separation zone appeared between the immediate roof and the main roof because of differential subsidence (Fig. 7c). At the 10th step, the mine face had advanced 100 m, the main roof has caved completely, and fractures continued to develop upward to a height of ≈45 m (Fig. 7d). When the excavation was 120 m long, the roof's failure length increased to ≈65 m.

When the mined length reached 20 m, a small amount of groundwater inflow from the coal seam floor occurred, most probably due to the presence of fissured siltstone, and mining was not significantly affected. Concurrently, a ≈7 m long fracture developed at the top of the Ordovician limestone (Fig. 8a). When the coal seam floor failure reached the 2 m thick limestone, groundwater inflow from the limestone into the mine increased, but the total water quantity was still small. Additionally, the damage zones expanded horizontally due to additional seepage of water from the thin limestone (Fig. 8b). When the depth of coal seam floor failure reached the Xu limestone, the seepage channel broadened and the key damage zone has additional water flow paths. However, the Ordovician limestone was still not affected. Therefore, the inflow was still too small to threaten mining operations (Fig. 8d). When the floor failure depth subsequently increased and the damaged zone crossed into the Cao limestone, groundwater inflow from the roof also entered the mined space (Fig. 8e). The depth of the floor failure kept increasing until it reached fractures that were hydrologically connected with the Ordovician limestone. At this point, new groundwater inflow pathways formed and flooding from the Ordovician aquifer began (Fig. 8f). Water rushed in, as described previously, at the 127 m excavation (Fig. 2), which was generally consistent with this simulation.

Discussion

The RFPA^{2D}-FLOW numerical simulation revealed the evolution of the fracture systems during mining through fracture generation, extension, broadening, and coalescence. The fracture process starts with the formation of a dominant fracture at an angle of ≈70° with the horizontal at the left end of the excavation. This initial fracture played a key role in the development of a complex fracture system, delineating a damage zone that provided flow paths for the groundwater.

Despite the fact that the depth of coal seam floor failure is usually greater in shallow mines than in deep mines with high ground stress conditions, the reverse trend has also been noticed (Jiang 2009). This abnormal trend was also identified in the current study. The modeling failure depth was ≈50 m, which is greater than found in previous studies. The major reasons for the coal seam floor failure were: (1) high original vertical ground stress, ranging from 25.55 to 25.63 MPa at a mining depth of almost 1000 m, according to the in situ test results at the 7192 roadway (Kang et al. 2007); (2) high underground pressure, with the ratio of underground pressure to original vertical ground stress ranging from 2 to 5 (Kang 2013)—we used the average value of 3.5 to estimate the underground pressure as almost 89.43 MPa, which in the presence of the 8 m thick siltstone and 17 m thick relatively medium-fine sandstone, prevented the roof from collapsing and also

produced arc- and shell-like stress fields (Fig. 6c–f); (3) the presence of mechanically weaker aquitards (mudstone, claystone, and argillaceous siltstone under the coal seam) with compressive strengths ranging from 23.0 to 45.0 MPa, with an average of 35.9 MPa (Table 2); and (4) the width of the working face, which was about 130 m at the no. 4196 west working face; the wider the face, the greater the coal seam floor failure depth (Xu and Yang 2013).

Even though the confined Xu and Cao limestone aquifers lie between the Ordovician limestone and the mined seam, they are thinner and have less water capacity. When the damaged zone connected with these aquifers, groundwater flowed upward through the newly created fractures at a rapid rate because of the increased permeability (Pang et al. 2014; Yang et al. 2007). The potential energy of groundwater confined under pressure was transformed into kinetic energy (Li et al. 2009a, b), contributing to fracture erosion and expansion (Feng et al. 2006) until it eventually modified the overall permeability and resistance of the rocks under the coal seam. This behavior was influenced both by the density of pre-mining fractures and rock permeability. Our modeling shows that the dominant fracture grew faster, eventually becoming the main flow path for groundwater inflow. Pre-mining fractures, especially those at the top of the Ordovician limestone, also affected the resistance of the overlying rocks. Once both the pre-mining and mining-induced flow paths connected to the Ordovician limestone, groundwater flow accelerated and flooding occurred.

Describing the evolution of groundwater flow paths by numerical simulation also allowed us to identify the place and time of most concern with respect to flooding into a deep mine where longwall extraction is employed. As mining advances, failure depth grows gradually from fracture generation, extension, broadening, and connection until the groundwater flow paths are completely connected and water inrush occurs. At this point, the excavation length is equal to the width of the working face. The weak floor strata can support only a minimal load and, when the rock strength is exceeded, the potential for damage and failure is great (Kong et al. 2012; Qian et al. 1995). This is similar to what occurs during "goaf square of the longwall face", which can produce abnormal strata pressures and very fierce ground behaviors (Kong et al. 2012).

To better constrain the depth of floor failure, water injection tests were conducted in one bore hole at the no. 7191 working face (Fig. 2b), a location with similar geological and hydrogeological conditions as those found at the no. 4196 west working face. The water injection test measured the injected water leaks at different depths in the borehole using drilling equipment capable of double end seal leak detection (Shi et al. 2005). The details of the method and in situ test data acquisition and processing were described previously (Yin 2005). The low pre-mining hydraulic conductivities and permeability increased after excavation and the maximum failure depth was almost 45 m, which is consistent with the results of our numerical modeling, except that in the former, no groundwater inrush occurred.

Therefore, in order to prevent flooding in the Panxi coal mine, the mining methods will have to be changed. Options to prevent flooding include: (1) reducing the mining width; (2) employing double-face mining; (3) mining followed by filling; (4) surface mining; (5) caving the roof artificially (Zhang 2005); and (6) grouting to strengthen the mechanical properties of the aquitards in the coal seam floor or transform the thin aquifers into aquifuges to resist the water and underground pressure. Further measures could also include lowering the hydraulic head of the confined aquifers by dewatering to reduce the water pressure on the strata overlying the aquifers.

Conclusions

We investigated the deformation and failure characteristics of floor strata in a deep longwall coal mine using numerical analysis. The numerical simulation predicted the temporal and spatial evolution of groundwater flow paths under the mine excavation and showed that, under the conditions considered, the failure depth of the floor strata was reached at $\approx$50 m. This is the first study to discuss the abnormal characteristics of the floor failure depth in a deep longwall coal mine. The main factors that affect the development of the groundwater flow path are: (1) the high ground stress and underground pressure in a deep mine; (2) the large width of the working face; (3) the excavation length; (4) the presence of softer rocks under the coal seam floor; (5) fracture erosion by groundwater from thin aquifers; and (6) pre-mining fractures present at the top of the Ordovician limestone.

It is critically important to determine the time and location of the maximum probability of groundwater flooding in a deep longwall coal mine, as this information is the critical to understanding and preventing flooding when the mining length is the same as the width of the large working face. The results presented in this case study may be useful in other mining operations with similar conditions as those considered in this study.

Acknowledgments This research was financially supported by: the National Basic Research Program of China (973 Project, Grant 2012CB723104), the National Nature Science Foundation of China (Grants 41372290 and 41402250), the National Nature Science Foundation of Shandong Province (Grant ZR2013EEQ 019), the State Key Laboratory of Mining Disaster Prevention and Control (Grant MDPC2012KF13), and the innovative research team of Shandong

University of Science and Technology (Grant 2012KYTD101). The authors also thank the technicians in the Department of Geology and Survey in Panxi coal mine for their data collection, and the anonymous reviewers and the editors for their helpful suggestions.

References

Feng Q, Yang T, Yu Q, Tang C, Feng X (2006) Numerical simulation on water inrush from the seam floor based on the coupled analysis of seepage and damage. J Saf Environ 3:1–4

Gu X, Wang J, Liu Y (2010) Water resistant features of high-risk outburst coal seams and standard discriminant model of mining under water-pressure. Min Sci Technol 20:797–802

He M, Xie H, Peng S, Jiang Y (2005) Study on rock mechanics in deep mining engineering. Chin J Rock Mech Eng 16:2803–2813

Huang Z, Jiang Z, Qian Z, Cao D (2014a) Analytical and experimental study of water seepage propagation behavior in the fault. Acta Geodyn Geomater 176:361–370. doi:10.13168/agg.2014.0017

Huang Z, Jiang Z, Zhu S, Qia Z, Cao D (2014b) Characterizing the hydraulic conductivity of rock formations between deep coal and aquifers using injection tests. Int J Rock Mech Min Sci 71:12–18. doi:10.1016/j.ijrmms.2014.06.017

Jiang Q (2009) Coal floor strata failure depth test of working face at big mining depth. J Coalfield Geol Explor 4:30–33

Jin D, Zheng G, Liu Z, Liu Y, Pang X (2011) Real-time monitoring and early warning techniques of water inrush through coal floor. Proc Earth Planet Sci 3:37–46

Kang H (2013) Stress distribution characteristics and strata control technology for roadways in deep coal mines. Coal Sci Technol 9:12–17

Kang H, Lin J, Zhang X (2007) Research and application of in situ stress measurement in deep mines. Chin J Rock Mech Eng 5:929–933

Kong L, Qi Q, Jiang F, Ouyang Z (2012) Abnormal strata stress resulted from goaf square of longwall face based on microseismic monitoring. Chin J Rock Mech Eng 2:3879–3896

Li L, Xu T, Tang C, Zhu L (2007) Numerical simulation of creep induced progressive failure process of rock under uniaxial compression. Rock Soil Mech 9:1978–1982

Li L, Tang C, Ma T (2008) Research on the closure and creep mechanism of circular tunnels. J Coal Sci Eng 2:195–199

Li L, Tang C, Li G, Yang T (2009a) Damage evolution and delayed groundwater inrush from micro faults in coal seam floor. Chin J Geotech Eng 12:1837–1844

Li L, Tang C, Liang Z, Ma T, Zhang Y (2009b) Numerical analysis of pathway formation of groundwater inrush from faults in coal seam floor. Chin J Rock Mech Eng 2:290–297

Li H, Bai H, Jiao Y, Yang C (2013) Water injection test and numerical analysis of the mining-induced failure depth of floor. Electron J Geotech Eng 18(1):849–857

Li L, Zhou Z, Li S, Xue Y, Xu Z, Shi S (2014) An attribute synthetic valuation system for risk assessment of floor water inrush in coal mines. Mine Water Environ. doi:10.1007/s10230-014-0318-0

Mahdi S, Charliec L (2012) Numerical modeling of longwall mining and stability analysis of the gates in a coal mine. Int J Rock Mech Min Sci 51:24–34. doi:10.1016/j.ijrmms.2012.02.002

Pang Y, Wang G, Ding Z (2014) Mechanical model of water inrush from coal seam floor based on triaxial seepage experiments. Int J Coal Sci Technol 4:428–433. doi:10.1007/s40789-014-0049-7

Qian M, Miao X, Li L (1995) Mechanism of fracture behavior of main floor in longwall mining. Chin J Geotech Eng 6:55–62

Shi L, Zhu L, Han J, Su B, Yin W, Li G (2005) Monitor study on broken floor depth caused by underground pressure. Coal Geol Explor 6:20–23

Tang C, Tham L, Lee P, Yang T, Li L (2002) Coupling analysis of flow, stress and damage (FSD) in rock failure. Int J Rock Mech Min Sci 4:477–489. doi:10.1016/S1365-1609(02)00023-0

Wang J, Park H (2003) Coal mining above a confined aquifer. Int J Rock Mech Min Sci 40:537–551. doi:10.1016/S1365-1609(03)00029-7

Wang S, Sloan S, Sheng D, Tang C (2012a) Numerical analysis of the failure process around a circular opening in rock. Comput Geotech 39:8–16. doi:10.1016/j.compgeo.2011.08.004

Wang Y, Yang W, Li M, Liu X (2012b) Risk assessment of floor water inrush in coal mines based on secondary fuzzy comprehensive evaluation. Int J Rock Mech Min Sci 52:50–55. doi:10.1016/j.ijrmms.2012.03.006

Wu Q, Liu Y, Liu D, Zhou W (2011) Prediction of floor water inrush: the application of GIS-based AHP vulnerable index method to Donghuantuo Coal Mine, China. Rock Mech Rock Eng 44:591–600. doi:10.1007/s00603-011-0146-5

Wu Q, Fan S, Zhou W, Liu S (2013) Application of the analytic hierarchy process to assessment of water inrush: a case study for the no. 17 coal seam in the Sanhejian Coal Mine, China. Mine Water Environ 32:229–238. doi:10.1007/s10230-013-0228-6

Xie G, Chang J, Yang K (2009) Investigations into stress shell characteristics of surrounding rock in fully mechanized top-coal caving face. Int J Rock Mech Min Sci 46:172–181. doi:10.1016/j.ijrmms.2008.09.006

Xu Y, Yang Y (2013) Application analysis on statistical formula for failure depth of coal seam floor in deep mine. Coal Sci Technol 9:129–132

Yang T, Liu ZhuW, Elsworth D, Tham L, Tang C (2007) A coupled flow-stress-damage model for groundwater outbursts from an underlying aquifer into mining excavations. Int J Rock Mech Min Sci 44:87–97. doi:10.1016/j.ijrmms.2006.04.012

Yang W, Lin B, Qu Y, Li Z, Zhai C, Jia L, Zhao W (2011) Stress evolution with time and space during mining of a coal seam. Int J Rock Mech Min Sci 48:1145–1152. doi:10.1016/j.ijrmms.2011.07.006

Yin H (2005) Study of water-inrush mechanism and prediction of coal bed floor in Pan-xi coal field. Shandong University of Science and Technology, Qingdao, pp 36–38

Yin H, Wei J, Li Z, Shi L (2007) Analysis on water inrush mechanism in fracture tectonics of Panxi coalmine. J Shandong Univ Sci Technol 1:30–33

Zhang J (2005) Investigations of water inrushes from aquifers under coal seams. Int J Rock Mech Min Sci 42:350–360. doi:10.1016/j.ijrmms.2004.11.010

Zhu S, Jiang Z, Zhou K, Peng G, Yang C (2014) The characteristics of deformation and failure of coal seam floor due to mining of the Xinmin coal mine in China. Bull Eng Geol Environ 73:1151–1163. doi:10.1007/s10064-014-0612-x